Dyes and Pigments 168 (2019) 103–110

Contents lists available at ScienceDirect

Dyes and Pigments

journal homepage: www.elsevier.com/locate/dyepig

Synthesis, characterization and application of *meso*-substituted fluorinated boron dipyrromethenes (BODIPYs) with different styryl groups in organic photovoltaic cells

António Aguiar[a], Joana Farinhas[b], Wanderson da Silva[a], Mariana Emilia Ghica[a], Christopher M.A. Brett[a], Jorge Morgado[b,c], Abílio J.F.N. Sobral[a,*]

[a] Chemistry Department, FCTUC, University of Coimbra, 3004-535, Coimbra, Portugal
[b] Instituto de Telecomunicações, Instituto Superior Técnico, Av. Rovisco Pais 1, P-1049-001, Lisboa, Portugal
[c] Department of Bioengineering, Instituto Superior Técnico, University of Lisbon, Av. Rovisco Pais 1, P-1049-001, Lisboa, Portugal

ARTICLE INFO

Keywords:
BODIPY dyes
Small molecules
Optoelectronic properties
Organic photovoltaic cells
Photovoltaic performance

ABSTRACT

A series of highly fluorinated BODIPY dyes with different styryl aromatic donor groups such as phenyl, naphthyl and anthracyl were designed, synthesized, characterized and applied as electron-donor materials in organic photovoltaic cells (OPV). The introduction of the styryl moieties leads to a large bathochromic shift and to a significant decrease in the HOMO-LUMO energy-gaps. All the BODIPY dyes showed relatively low HOMO energies ranging from −5.21 to −5.54 eV as determined from cyclic voltammetry measurements. Furthermore, they all show good solubility in organic solvents, thermal stability, excellent film-forming abilities which added with the great optoelectronics characteristics makes them excellent candidates as electron-donor materials for OPV cells. The power conversion efficiency (PCE) of the OPV based on the best BODIPY blend (BDP3/$PC_{70}BM$ (1:2, w/w) was 2.8% with a high open circuit voltage (V_{OC}) of 1.00 V, which is a very promising PCE result for BODIPY based OPV and a top V_{OC} value for this kind of systems.

1. Introduction

Over the last 3 decades organic photovoltaic cells (OPV) have driven an intense research effort aiming at obtaining new materials that could push the power conversion efficiency up, eventually reaching values comparable to those of the silicon solar cells. Although the power conversion efficiencies of OPV have not, this far, exceeded 13% and material stability remains a challenge, this sort of photovoltaic device presents strong advantages, such as simple preparation, lightweight, flexibility and low-cost fabrication [1–5].

The use of pyrrolic small molecules, such as porphyrins or phthalocyanines, or even pyrrolic moieties on polymers backbones, in OPV, has been quite widely studied since such molecules are among the most efficient electron-donor materials in bulk heterojunction (BHJ) OPV [6–8]. Compared with the polymeric counterparts, small molecules are synthesized with accurate molecular weight, better-defined structures and better reproducibility and are easier to purify [9–11].

In contrast to other pyrrolic compounds, the boron dipyrromethene (BODIPY) dyes have not been studied with the same consistency by the OPV community. In addition to their molecular versatility (as they can be functionalized at all positions of the core), BODIPY dyes have great potential to be applied in OPV since they combine strong absorption coefficient in the visible and near-IR ranges, relatively long excited-state lifetime, good solubility in organic solvents, good photo and thermal stability, suitable HOMO and LUMO energy levels to ensure efficient charge separation upon blending with a fullerene acceptor, extended π-electron delocalization and offer the possibility to increase the π-electron delocalization by post-functionalization [8,12–17].

Herein we report the synthesis and assessment of the optical and electrochemical properties of a series of highly fluorinated BODIPY dyes. Highly fluorinated BODIPY dyes are expected to combine several advantageous features, such as high stability and prominent spectroscopic properties. The fluorine atoms enhance the electron-acceptor character of the moiety they are bound to [18]. This electron-withdrawing effect of the fluorine atoms, move the HOMO and LUMO levels down in energy, which could improve the open voltage circuit (V_{OC}), should the dye be used as electron-donor material. It was reported that upon photoexcitation the charge density at the *meso*-position of BODIPY dyes increases, while at the other positions of the BODIPY system it decreases [19]. Based on this intrinsic asymmetry in the charge

* Corresponding author.
E-mail address: asobral@ci.uc.pt (A.J.F.N. Sobral).

https://doi.org/10.1016/j.dyepig.2019.04.031
Received 28 February 2019; Received in revised form 12 April 2019; Accepted 13 April 2019
Available online 22 April 2019

redistribution of excited BODIPY dyes, we designed D-π-A structured BODIPY sensitizers in which a pentafluorophenyl group is introduced at *meso* position, and electron-donating groups are introduced at the α-pyrrolic position via the Knoevenagel condensation to generate styryl-substituted BODIPY dyes. Among the few reported works using BODIPYs derivatives as electron-donor species in OPV [20–29], to the best of our knowledge, this is the first work reporting this type of D-π-A structured BODIPY chromophores with a pentafluorophenyl group introduced at the *meso* position. With the introduction of distyryl moieties (phenyl, naphthyl or anthracyl groups) we found a significantly broad absorption spectrum, improving the light-harvesting ability in the entire sunlight region and a decrease of the HOMO-LUMO energy-gap (E_g). The photophysical and electrochemical properties of these dyes were deeply studied, revealing the relationships between the structures and the photovoltaic characteristics and results. The synthesized BODIPY were used as electron-donor materials in blends with either $PC_{60}BM$ or $PC_{70}BM$, and the photovoltaic performance of the cells and the morphology of the films were investigated in detail.

2. Experimental

2.1. Materials and reagents

Reagents and solvents were obtained from Sigma-Aldrich and used without further purification. Solvents for photophysical studies were HPLC grade (CHROMASOLV plus) purchased from Sigma-Aldrich. Analytical thin layer chromatography (TLC) was performed on Merck silica gel plates with F-254 indicator. For visualization, a twin wavelength ultraviolet lamp (254 and 365 nm) was used. Silica gel column chromatography was carried out with silica gel (230–400 mesh) from Fluka.

2.2. Equipments

^{1}H, ^{19}F and ^{13}C spectra were recorded on a Bruker AVANCE III NMR (operating at 400.15 MHz for proton, and 100.63 MHz for carbon atoms) NMR spectrometers with TMS as the internal reference and $CDCl_3$ as solvent. Chemical shifts (δ) are quoted in ppm relative to TMS. Coupling constants (J) are presented in Hz. Electronic absorption spectra were recorded on a Jasco V-530 double-beam UV/Vis spectrometer, using 1 cm path length quartz cells. Steady-state fluorescence studies were carried out using a Horiba-Jobin-Yvon SPEX Fluorolog 3–22 spectrometer. Fluorescence spectra were made by using optically dilute solutions and were automatically corrected for the wavelength response of the system. UV–Vis spectra films were measured with a Helios Gamma spectrophotometer. Cyclic voltammetric (CV) measurements for dyes were carried out with a computer controlled Ivium Compact Stat, in a one-compartment three electrode system consisting of a glassy carbon electrode (GCE) (geometric area 0.00785 cm^2) working electrode, a platinum wire as counter electrode and an Ag/AgCl (3 M KCl) as reference electrode at a scan rate of 50 mV s^{-1}. The supporting electrolyte was tetrabutylammonium tetrafluoroborate (TBATFB, 0.1 M) in anhydrous dichloroethane (CH_2Cl_2). The results were calibrated using a 1 mM ferrocene/ferrocenium (Fc/Fc+) redox couple as internal standard. CV experiments were carried out using 1 mM concentrations of each BODIPY studied. UV/Vis absorption spectra of the films were recorded in a Cecil 7200 spectrophotometer. Thermogravimetric analyses (TGA) were conducted under a dry nitrogen gas flow at a heating rate of 20 °C/min on a Parkin-Elmer STA 6000 instrument. Differential scanning calorimetry analyses were conducted on Netzsch DSC 200F3 instrument. Film thicknesses were measured with a Dektak 6 M profilometer. AFM studies were performed on a Nano Observer from Concept Scientific Instruments (LesUlis, France), operating in noncontact mode, with cantilevers having a resonance frequency between 200 and 400 kHz and silicon probes with tip radius smaller than 10 nm. High resolution ESI positive mode mass spectra were obtained on a QqTOF Impact II™ mass spectrometer (Bruker Daltonics) operating in the high-resolution mode. Samples were analysed by flow injection analysis (FIA) using an isocratic gradient 30 A:70 B of 0.1% formic acid in water (A) and 0.1% of formic acid in acetonitrile (B), at a flow rate of 10 μLmin-1 over 15 min. The TOF analyser was calibrated in the *m/z* range 100–1500 using an internal calibration standard (tune mix solution) which is supplied from Agilent. The full scan mass spectra were acquired over a mass range of 100–1350 *m/z* at a spectra rate of 1 Hz.

2.3. OPV manufacture and characterization

The photovoltaic devices were prepared on glass substrates coated with 100 nm thick Indium−Tin-Oxide (ITO). They were cleaned under ultrasound with distilled water and a non-ionic detergent, followed by distilled water, acetone, isopropyl alcohol and then dried under N_2 flow. The ITO surface was then cleaned under UV-oxygen plasma for 3 min prior to depositing, by spin coating, a 40 nm thick layer of poly (3,4-ethylenedioxythiophene):polystyrene sulfonic acid (PEDOT:PSS) (Clevios P VP. AI 4083, from Heraeus) which was then dried on a hot plate at 125 °C for 10 min. The solutions of the blends were spin-coated (1300 rpm, 60 s) on top of PEDOT:PSS in air. The thickness of the blend films was measured with a profilometer (DEKTAK 6 M). Following the deposition of the active blend films, Ca (20 nm) and Al (80 nm) were thermally evaporated on top, under a base pressure of 10^{-6} mbar, defining a device area of 0.24 cm^2. The current-voltage characteristics of the photovoltaic cells were measured under inert atmosphere (N_2) using a Keithley 2400 source-measure unit. The curves under illumination were measured with a solar simulator with simulated AM1.5G illumination at 85–93 mW/cm^2 (Oriel Sol 3 A, 69920, Newport). At least 16 devices of each condition were prepared. The light intensity of the solar simulator was verified using a calibrated solar cell. External quantum efficiency (EQE) spectra were obtained under short-circuit conditions, using a homemade system with a halogen lamp as light source.

2.4. Synthesis

2.4.1. Synthesis of BDP1

BDP1 was prepared according to procedures described previously, using pentafluoro benzaldehyde and 3-ethyl-2,5-dimethyl-pyrrole as starting reagents [30]. **^{1}H NMR (400 MHz, $CDCl_3$) (ESI Fig. S1)** δ (ppm): 2.54 (s, 6H), 2.33 (q, J = 7.6 Hz, 4H), 1.51 (s, 6H), 1.02 (t, J = 7.6 Hz, 6H **^{19}F NMR (376 MHz, $CDCl_3$) (ESI Fig. S2)** δ (ppm): 139.23 (m, 2 F), 145.74 (m, 2 F), 151.11 (m, 1 F), 159.89 (m, 2 F); **^{13}C NMR (100 MHz, $CDCl_3$) (ESI Fig. S3) δ (ppm):** 156.15; 144.2 (d, J = 250.52 Hz); 141.94 (d, J = 262 Hz); 138.19 (d, J = 257.86 Hz); 136.58; 133.91; 130.36; 121.16; 110.32 (td, J = 19.44, 4.03 Hz); 17.09; 14.54; 12,74 (t, J = 2.57 Hz); 10.85. **Elemental Analysis** Calculated for $C_{23}H_{22}BF_7N_2$: C,58.75; H, 4.72; N, 5.96; Found: C,58.81; H, 4.72; N, 5.65;

All the following BODIPY synthesis procedures were based on some reported work [19,31–34], but due to the strong capability to suffer nucleophilic substitution at *para* position of pentafluorophenyl moiety they were optimized as described below.

2.4.2. Synthesis of BDP2

BDP1 (250 mg; 0.54 mmol), 12.5 mg of *p*-TsOH.H_2O, 0.55 mL of benzaldehyde (5.5 mmol) and 0.50 g of 4 Å molecular sieves were added to a 50 mL round-bottom flask. The round-bottom flask was then degassed and refilled with N_2 three times followed by the addition of 15 mL of toluene and 0.25 mL of piperidine, and this mixture was refluxed for 2 h. The mixture was washed with water several times, the organic phase solvent was removed under vacuum, and the obtained solid was purified by column chromatography on silica gel eluting with DCM-hexane (v/v 1:1) and preparative TLC using DCM-hexane (v/v 4:6). **BDP2** (109 mg; 31% yield) was obtained as deep-blue solid.

BDP2: ^{1}H NMR (400 MHz, $CDCl_3$) (ESI Fig. S4) δ (ppm): 7.77 (d, J = 16.8 Hz, 2H), 7.64 (d, J = 7.6 Hz, 4H), 7.42 (t, J = 7.6 Hz, 4H), 7.38–7.28 (m, 4H), 2.66 (q, J = 7.6 Hz, 4H), 1.57 (s, 6H) 1.21 (t, J = 7.6 Hz, 6H); **^{19}F NMR (376 MHz, $CDCl_3$) (ESI Fig. S5)** δ (ppm): −138.63 to −138.77 (m, 2 F), −138.96 (dd, J = 66.4, 33.2 Hz, 2 F), −150.78 (t, J = 20.6 Hz, 1 F), −159.55 to −159.80 (m, 2 F); **^{13}C NMR (100 MHz, $CDCl_3$) (ESI Fig. S6) δ (ppm):** 152.07; 137.34; 137.09; 134,97; 132.82; 129.05; 128.84; 127.82; 127.58; 119.73; 29.71; 18.42; 14.06; 10.72. **HRMS (ESI Fig. S18) m/z [M + H]$^+$** calculated for $C_{37}H_{30}BF_7N_2^+$: 647.2463; Found: 647.2469.

2.4.3. Synthesis of BDP3

BDP1 (200 mg; 0.45 mmol), 10 mg of p-TsOH.H_2O, 0.7 g of 2-naphthaldehyde (4.5 mmol) and 0.50 g of 4 Å molecular sieves were added to a 50 mL round-bottom flask. The bottle was then degassed and refilled with N_2 three times followed by the addition of 15 mL of toluene and 0.25 mL of piperidine, and this mixture was refluxed for 2 h. The mixture was washed with water several times, the organic phase was evaporated, and purified by column chromatography on silica gel eluting with DCM-hexane (v/v 1:1) and preparative TLC using DCM-hexane (v/v 4:6). **BDP3** (67 mg; 36%) was obtained as a deep-blue solid.

BDP3: ^{1}H NMR (400 MHz, $CDCl_3$) (ESI Fig. S7) δ (ppm): 7.98–7.82 (m, 12H), 7.55–7.46 (m, 6H), 2.72 (q, J = 7.7 Hz, 4H), 1.60 (s, 6H) 1.30–1.24 (m, 6H); **^{19}F NMR (376 MHz, $CDCl_3$) (ESI Fig. S8) δ (ppm):** −138.55 to −139.00 (m, 4 F), 150.76 (t, J = 20.6 Hz, 1 F), 159.69 (dt, 22.5, 6.9 Hz, 2 F)); **^{13}C NMR ($CDCl_3$) (ESI Fig. S9) δ (ppm):** 152.05; 137.47; 137; 06; 135.15; 134.72; 133.80; 133.02; 128.60(d; 4.03 Hz); 128.38(d; 4.03 Hz); 127.83; 126.66; 126.53; 123.78; 120.00; 29.71; 18.52; 14.12; 10.74; **HRMS (ESI Fig. S19) m/z [M + H]$^+$** calculated for $C_{45}H_{34}BF_7N_2^+$: 747.2776; Found: 747.2778.

2.4.4. Synthesis of BDP4

BDP1 (200 mg; 0.45 mmol), 10 mg of p-TsOH.H_2O, 1.4 g of 9-anthracenecarboxaldehyde (9 mmol) and 0.50 g of 4 Å molecular sieves were added to a 50 mL round-bottom flask. The round-bottom flask was then degassed and refilled with N_2 three times followed by the addition of 15 mL of toluene and 0.25 mL of piperidine, and this mixture was refluxed for 2 h. The mixture was washed with water several times, the organic phase was separated, and the solvent evaporated. The obtained solid was purified by column chromatography on silica gel eluting with DCM-hexane (v/v 1:1) and preparative TLC using DCM-hexane (v/v 4:6). **BDP4** (60 mg; 19%) was obtained as a deep-blue solid.

BDP4: ^{1}H NMR (400 MHz, $CDCl_3$) (ESI Fig. S10) δ (ppm): 8.45–7.37 (m, 6H), 8.32 (d, J = 17.00 Hz, 2H) 7.43–7.32 (m, 6H), 2.83 (q, J = 7.7 Hz, 4H), 1.68 (s, 6H), 1.33 (t, J = 7.7 Hz, 6H); **^{19}F NMR (376 MHz, $CDCl_3$) (ESI Fig. S11)** δ (ppm): −138.20–138.80 (m, 4 F), 150.54 (t, J = 20.6 Hz, 1 F), 159.50 (dt, 21.2, 6.9 Hz, 2 F); **^{13}C NMR ($CDCl_3$) (ESI Fig. S12) δ (ppm):** 151.99; 137.29; 135.28; 134.60; 132.96; 132.08; 131.44; 129.71; 128.70; 127.76; 126.22; 125.70; 125.26; 29.71; 18.60; 14.61; 10.89; **HRMS (ESI Fig. S20) m/z [M + H]$^+$** calculated for $C_{53}H_{38}BF_7N_2^+$: 847.3089; Found: 847.3102.

3. Results and discussion

3.1. Synthesis and structural characterization

BDP1 was chosen as reference for this work since its pentafluorophenyl substituent is a strong electron-acceptor moiety which affects, albeit lightly, its photophysical and electronic properties, at variance with BODIPY having some other *meso* substitution groups [35,36]. To the best of our knowledge no OPV cell studies were done with BODIPYs with this sort of acceptor moieties. The phenyl, naphthyl or anthracyl groups were attached by the Knoevenagel condensation reaction, catalysed by piperidine and p-toluenesulfonic acid (Scheme 1). This kind of reaction on BODIPYs can exceed 48 h of reaction time and normally does not have high yields but in our case the reaction time did not exceed 2 h until all the **BDP1** had been consumed. This is due to the strong electron-withdrawing feature imposed by the pentafluoro fraction, which facilitates deprotonation of the methyl group at the α-position of pyrrolic groups [33].

All prepared BODIPY derivatives exhibit good solubility in common organic solvents such as dichloromethane, chloroform, dichlorobenzene, THF, and ethanol. The structure and the purity of the compounds was evaluated by ^{1}H, ^{19}F and ^{13}C NMR. The coupling constants for the olefinic hydrogens in **BDP2-4** is around 17 Hz, indicative of the *trans* stereochemistry of the olefin double bond.

The TGA and DSC techniques provide valuable information about the thermostability of the BODIPY derivatives. The TGA curves of all BODIPYs investigated are presented in Fig. 1, and the DSC curves are shown in Fig. S14. In the DSC experiments, the dyes were heated from 25 to 350 °C and then cooled to 25 °C, at a rate of 10 °C/min under nitrogen flow. The endothermic peaks for **BDP1-4** are at 204 °C, 229 °C, 300 °C, and 280 °C, respectively, which correspond to their melting temperatures. These values are similar to the values obtained by a melting point meter. Nevertheless, no exothermic peak is observed during the cooling process. The decomposition temperatures obtained from TGA curves, observed at 5% weight loss, are 256 °C, 285 °C, 333 °C, and 303 °C, respectively. These results confirm that all BODIPYs exhibit high thermal stability, with high melting temperatures, which is a good characteristic for OPV application.

3.2. Electronic absorption and photoluminescence

The normalized absorption spectra of BODIPY dyes (**BDP1-4**) in solution are depicted in Fig. 2, and the matching optical data are presented in Table 1. As shown in Fig. 2 and in Fig. S13, the absorption spectra of the studied BODIPYs, particularly of the functionalized ones (**BDP2-4**), cover the visible and NIR regions of the solar spectrum, which is a desired requirement for efficient organic photovoltaic cells. The absorption spectrum of **BDP1** is characterized by a strong S0−S1 (π-π*) transition at 544 nm with a higher energy vibronic shoulder at about 30 nm from the main peak and a weaker broad band around 395 nm arising from the S0−S2 (π-π*) transition. The **BDP2-4** absorption spectra exhibit a higher broadening of the absorption bands and a significant red-shift, compared with the absorption spectrum of **BDP1**, evidencing the effect of stepwise expansion of the π-system due to the attachment of the distyryl moieties. The first band, at around 300–450 nm, is assigned to a localized π-π* transition from the electron-donors fragments, such as phenyl, naphthyl and anthracyl. The occurrence of this new absorption bands masks the weaker absorption band attributed to the S0−S2 (π-π*) transition of the BODIPY core. The absorption bands at lower energy (at around 500–775 nm) is attributed to a S0−S1 (π-π*) transition. The broadening and the lack of structure of the band attributed to a S0−S1 transition of **BDP4** could be explained by a torsional motion around an equilibrium configuration [37].

All these dyes show high molar absorption coefficients in dichloromethane solution, ranging from 2.1 to 1.0×10^5 $M^{-1}cm^{-1}$, which confirms their excellent light harvesting ability.

The film absorption spectra show a clear bathochromic shift of the absorption maximum with considerable broadening of the peaks. The red shift and broadening relative to solution spectra are likely the result of strong π-π stacking of adjacent molecules, leading to strong intermolecular interactions and a planarization of the system, Fig. 2 (B).

Considerable fluorescence was observed in dichloromethane solutions of **BDP1-4** at room temperature (Fig. 2). The wavelengths at maximum emission are presented in Table 1, and the small Stokes shift is indicative of a reduced geometry reorganization between S1 and S0. Excitation of these compounds at their respective three absorption bands at room temperature resulted in the same emission wavelength band.

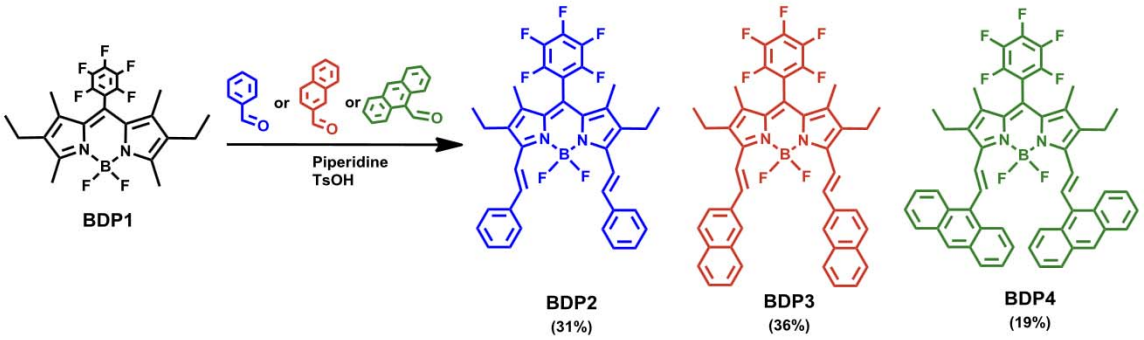

Scheme 1. The synthesis of the distyryl-BODIPY derivatives and their respective yields.

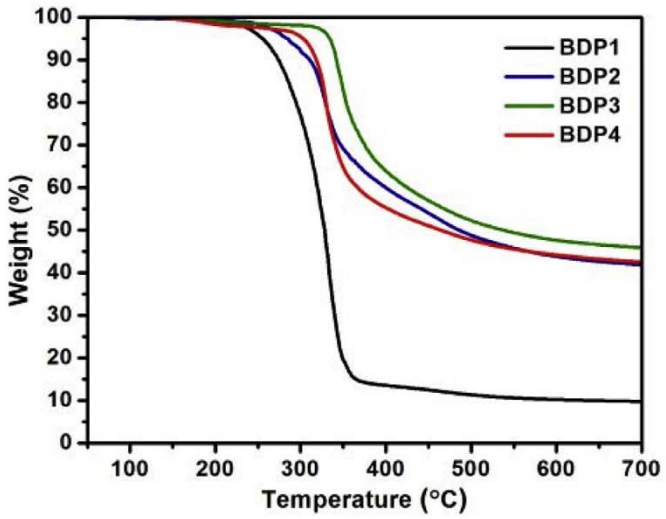

Fig. 1. TGA curves of **BDP1-4** recorded at a heating rate of 20 °C/min under nitrogen atmosphere.

3.3. Electrochemical properties

Cyclic voltammetry (CV) was used to study the electrochemical properties of the BODIPY dyes using 0.1 M TBATFB in dichloroethane as supporting electrolyte. The values of potential were standardized with ferrocene/ferrocenium (Fc/Fc^+) couple as internal reference vs. Ag/AgCl and it is assumed that the redox potential of Fc/Fc^+ has an absolute energy level of −4.80 eV in relation to vacuum. Dyes solutions were degassed with N_2 for 5 min before carrying out the CV measurements. The cyclic voltammograms of **BDP 1–4** are shown in Fig. 3 and the electrochemical data is summarized in Table 2. As shown in Fig. 3, the cyclic voltammograms of the compounds exhibited a quasi-reversible profile and the first oxidation potential (onset oxidation potential) was used to estimate the HOMO energy level.

Table 1
Photophysical properties of **BDP1-4**.

Entries	λ^{abs} (nm)[a]	ε (cm^{-1} M^{-1})	λ^{abs} (nm)[b]	λ^{em} (nm)[a]	Δν (cm^{-1})	Eg (eV) (onset)[a]
BDP1	544	5.0×10^4	551	559	493	2.19
BDP2	661	6.4×10^4	694	678	380	1.80
BDP3	681	1.0×10^5	725	697	337	1.73
BDP4	648	2.1×10^4	678	690	940	1.70

E_g = estimated from the absorption spectra onset of dyes in CH_2Cl_2.
[a] In CH_2Cl_2 solution.
[b] In film.

The oxidation potential of the parent compound, **BDP1**, is slightly higher than that of the derivatives **BDP2, BDP3** and **BDP4** (Table 2). The onset oxidation potential from derivative compounds shifts to a less positive value accompanied by a peak current increase confirming that the functionalization did indeed induce a stronger electron-donor character to the new compounds. It is also observed that the different distyryl moieties (phenyl, naphthyl and anthracyl) did not have a pronounced shifting effect on the oxidation potentials. The dyes' HOMO and LUMO energy levels calculated from the electrochemical experiments and upon combination of the optical properties, respectively, are both above the HOMO and LUMO energies of $PC_{60}BM$ and $PC_{70}BM$, the electron-acceptor species selected to blend with the BODIPY dyes (Scheme 2) [38]. This means that the dye-fullerene combination forms a type II heterojunction, a feature that is essential to promote exciton dissociation at the donor (BODIPY species) and the acceptor (fullerene

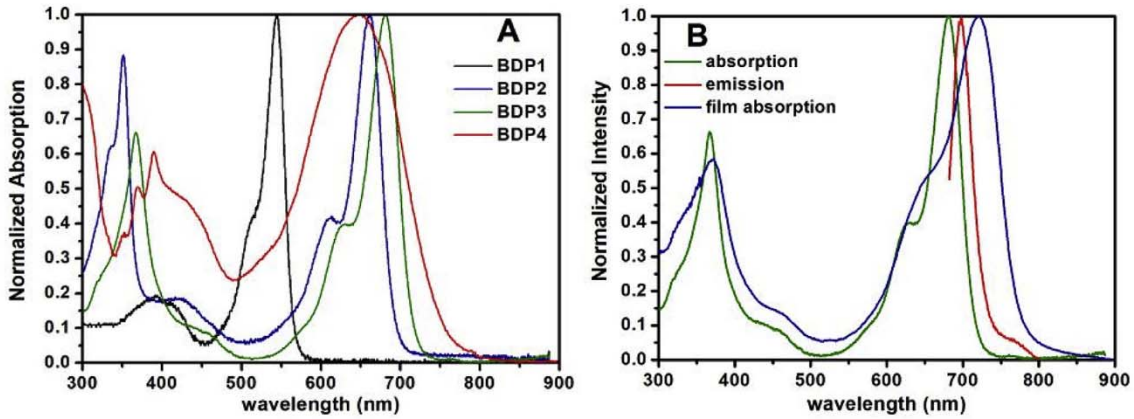

Fig. 2. Normalized absorption spectra of BODIPY series in CH_2Cl_2 solution (**A**) and comparison of normalized absorption, emission spectra of **BDP3** in CH_2Cl_2 solution and the normalized absorption in quartz film (**B**).

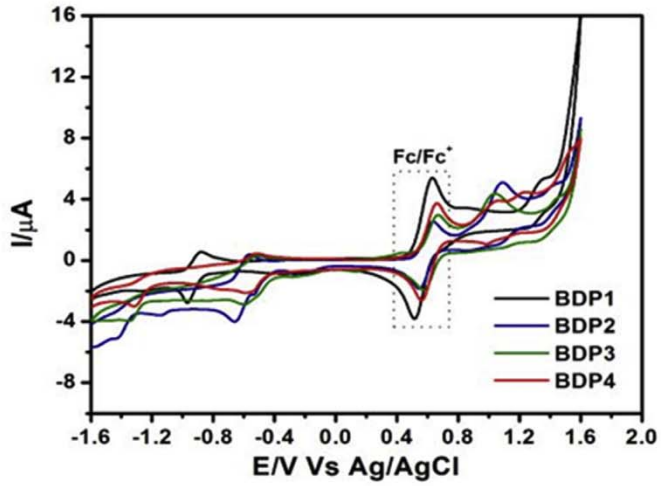

Fig. 3. Cyclic voltammograms of **BDP1-4,** at GCE in CH_2Cl_2 solution, containing 0.1 M TBATFB and 1 mM of the different BODIPY compounds in the presence of 1 mM ferrocene/ferrocenium (Fc/Fc^+) as internal standard, recorded at 50 mV s^{-1} in deoxygenated solution (N_2).

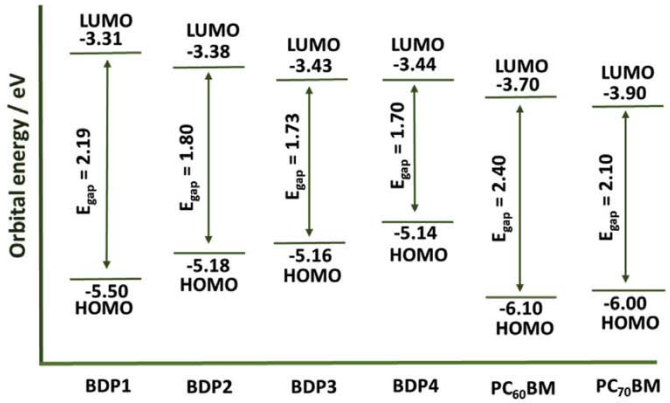

Scheme 2. Frontier orbital energy levels of the synthesized BODIPYs and the fullerenes derivatives $PC_{60}BM$ and $PC_{70}BM$.

species) interface. The difference in electron affinities creates a driving force at the interface between the two materials that is strong enough to separate the photogenerated excitons into charge carriers [2,39,40]. The constant increase of the HOMO level and the decrease of the LUMO level from **BDP1** to **BDP4** is a strong indication that the increase of aromaticity and donor ability from phenyl to anthracyl affects the optical electronics properties of the compounds. These results clearly demonstrate that these BODIPY dyes can be combined with either $PC_{60}BM$ or $PC_{70}BM$ to prepare organic solar cells.

3.4. Performance of the solar cells

All the presented BODIPYs show important properties such as: strong absorbance in the visible and NIR region of the solar spectrum, good solubility in organic solvents and suitable HOMO and LUMO energies to work as donor materials in a heterojunction with $PC_{60}BM$ or $PC_{70}BM$ in solar cells.

The solution processed bulk heterojunction organic photovoltaic cells were manufactured with the following structure ITO/PEDOT:PSS/active layer/Ca/Al. Firstly, the studied active layer was composed by BODIPY and $PC_{60}BM$ (electron-acceptor material). The PEDOT:PSS layer was spin-coated at 1800 rpm and dried for 10 min at a temperature of 125 °C to obtain a film thickness of about 40 nm.

To achieve the best power conversion efficiency (PCE) several optimization procedures, such as the donor:acceptor mass ratio, thermal annealing, thickness, solvent and blend solution concentration were investigated (Table S1).

The optimized BODIPY:$PC_{60}BM$ blend had a weight a ratio of 1:3, deposited by spin-coating at 1200–1300 rpm from a chloroform solution at 15 mg/ml, and thermally annealed of 100 °C for 10 min. This combination of condition led to active layers below 100 nm thickness.

The photovoltaic performance parameters are summarized in Table 3. Fig. 3 (A) shows the current-voltage (J–V) characteristics of the best performing solar cells. For the optimized conditions, the best PCE values were obtained for **BDP3** (1.05%) followed by **BDP2**, **BDP4** and **BDP1**. The lower PCE value for **BDP1** was expected due to the higher HOMO-LUMO energy gap, consistent with light absorption at shorter wavelength of the visible spectrum. The other 3 **BODIPYs** exhibit higher efficiencies, combining high short-circuit current (J_{sc}) and high open-circuit voltage (V_{oc}). Despite the relative low PCE values, the functionalized BODIPYs (**BDP2-4**) showed very reasonable V_{oc} values, compared with other BODIPY derivatives and even among various electron-donor materials [6,28,41]. The J_{sc} and FF values are related to light harvesting ability, recombination and charge transport and collection. Since the proposed BODIPY dyes present high absorption coefficients and broad absorbance in a favourable range of the spectrum, the low J_{sc} and FF values of this system could be due to a sub-optimal active layer morphology and/or to a poor charge transport. The PCE increases from the phenyl to naphthyl substitution (**BDP2** to **BDP3)** but then drops when the substituent size and π system extension increases with anthracyl substitution (**BDP4**). The highest photovoltaic efficiency of **BDP3** can be due to the highest absorption coefficient and to the fact that is the BODIPY that has the absorption bands more shifted to the infrared. **BDP4** is the worst performing dye among the functionalized BODIPYs. The anthracyl is more aromatic than naphthyl but, due to its size, makes communication between the BODIPY moiety and the PCBM acceptor more difficult, could lead to aggregate formation and, as Table 1 and Fig. 2 show, it has broader absorption bands but with lower intensity.

$PC_{60}BM$ is the most commonly used electron-acceptor material for OPV [42]. However, the low absorption of $PC_{60}BM$ in the visible range is a handicap. $PC_{70}BM$ has advantages over $PC_{60}BM$, since it shows stronger absorption in the visible region of the spectrum. We, therefore, have also studied the photovoltaic performance of the functionalized BODIPYs with $PC_{70}BM$.

Results are summarized in Table 3, confirming the positive effect of replacing $PC_{60}BM$ by $PC_{70}BM$. **BDP2**-based solar cells exhibit more than twice the current density and the PCE value improved by more than 5 times. For **BDP3**-based cells an improved efficiency is also observed. The use of $PC_{70}BM$ had, instead, a residual incremental effect on the PCE of **BDP4** cells. The V_{OC} of the better cell system is only a few

Table 2
Electrochemical properties of **BDP1-4**.

Entries	E_{red}^1 (V)	E_{ox}^1 (V)	E_{ox}^2 (V)	E_{onset}^{ox1} (V)	$E_{onset}^{Fc/Fc+}$ (V)	Eg^{opt} (eV)	E_{HOMO} (eV)	E_{LUMO} (eV)
BDP1	−0.97	1.35	1.53	1.21	0.51	2.19	−5.50	−3.31
BDP2	−0.66	1.08	1.41	0.91	0.53	1.80	−5.18	−3.38
BDP3	−0.59	1.03	1.43	0.89	0.53	1.73	−5.16	−3.43
BDP4	−0.56	1.05	1.23	0.87	0.53	1.70	−5.14	−3.44

Table 3
Photovoltaic parameters of the optimized BDP:$PC_{60}BM$ and BDP:$PC_{70}BM$ cells.

BODIPY		Donor:Aceptor ratio (w/w)	Active layer thickness (nm)	J_{SC} (mA/cm^2)	V_{OC} (V)	FF	PCE (%) max/avg[a]
BDP1	$PC_{60}BM$	1:3	87	0.13	0.37	0.27	0.01 (0.01)
BDP2		1:3	97	1.76	0.68	0.24	0.34 (0.29)
BDP3		1:3	96	3.86	0.84	0.29	1.05 (0.99)
BDP4		1:3	62	1.40	0.69	0.24	0.27 (0.27)
BDP2	$PC_{70}BM$	1:3	89	4.58	1.00	0.31	1.74 (1.64)
BDP3		1:3	81	5.88	0.93	0.29	1.87 (1.81)
BDP4		1:3	104	1.41	0.76	0.26	0.30 (0.29)
BDP3		1:1	127	5.03	0.78	0.30	1.33 (1.33)
BDP3		1:2	87	7.72	1.00	0.31	2.79 (2.55)

[a] Average values calculated from at least 8 devices.

hundredths of a volt lower than the highest in published work up until now for this sort of compounds and the values are on par with the state-of-the-art electron-donors.

BDP3 cells, which showed the better performance, were further investigated, in particular by changing the ratio of the blend. The best result was achieved with a BODIPY:$PC_{70}BM$ ratio of 1:2, and resulted in a big improvement in Jsc, and one of the best results for BODIPY-based OPV cells (PCE of 2.79%).

These results, despite preliminary and still requiring to be extended to all our compounds, illustrate the superior performance of the blend with $PC_{70}BM$ over the blend with $PC_{60}BM$, external quantum efficiencies (EQEs) were determined for **BDP3**:$PC_{70}BM$ and for **BDP3**:$PC_{60}BM$-based cells (Fig. 4 (D)). As displayed, the EQE profiles follow those of the blend films' absorption spectra. A broad response in the 300–800 nm spectral region is observed for both systems, the higher EQE of the $PC_{70}BM$-based cell being attributed to the larger $PC_{70}BM$ absorption in the visible region of the spectrum (Fig. 4 (C)).

3.5. Morphologies of the active layers

The morphology of the active layer (blend) is of great importance in OPV since it influences exciton dissociation and charge transport, thereby controlling the obtained photocurrent. Films of **BDP2**, **BDP3** and **BDP4** with $PC_{60}BM$ and $PC_{70}BM$ were characterized by AFM. As shown in Fig. 5, all films present very flat surfaces. The root mean squared (rms) roughness of the films of **BDP2**, **BDP3** and **BDP4** blended with $PC_{70}BM$ is slightly higher than the roughness of the corresponding films of the blends with $PC_{60}BM$. In addition to the low roughness, no significant phase separation is found (by the combination of topography and phase images), evidencing good miscibility between the BODIPY and the fullerenes, which is in general a requirement for efficient photovoltaic cells. It should be kept in mind, however, that the surface

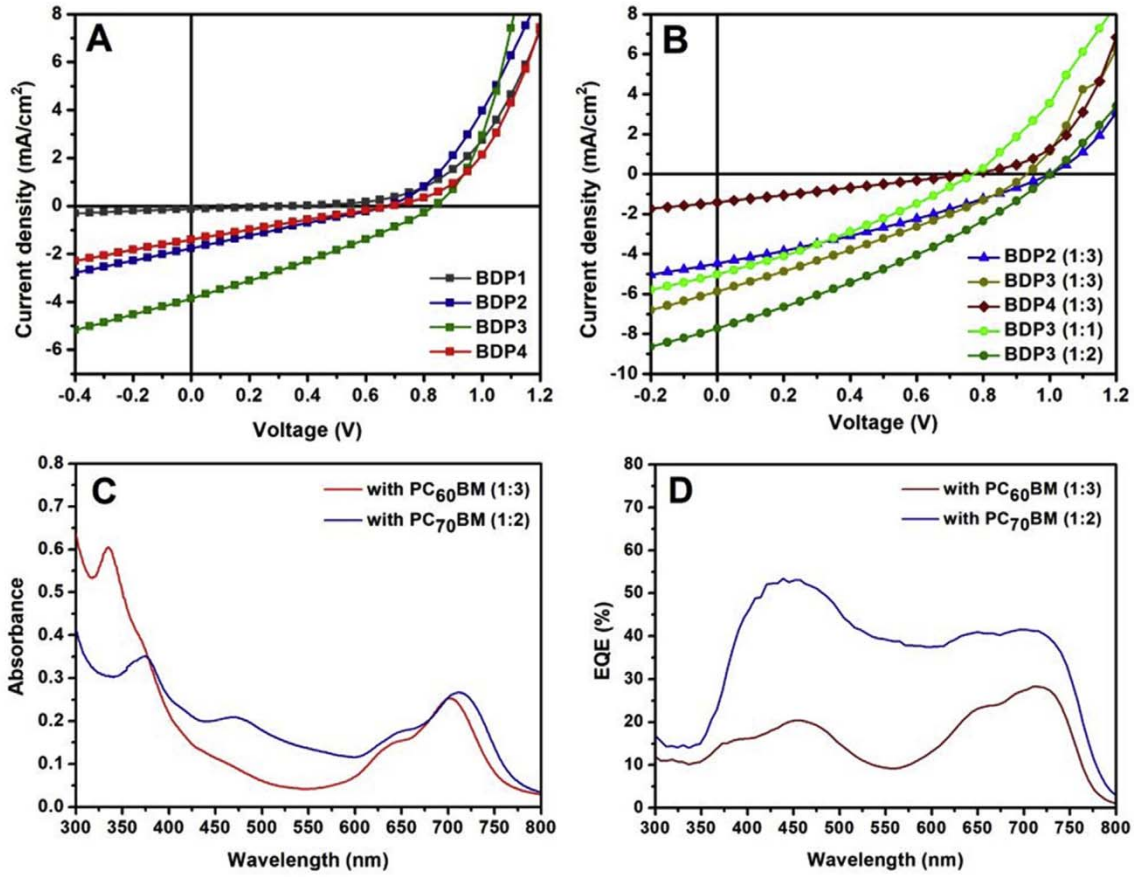

Fig. 4. Current density-voltage characteristics of **BDP1-4**:$PC_{60}BM$ based OPV cells (A) and of **BDP2-4**:$PC_{70}BM$ cells (B); absorption spectra (C) and EQE curves (D) of the optimized **BDP3**:$PC_{60}BM$ and **BDP3**:$PC_{70}BM$ systems.

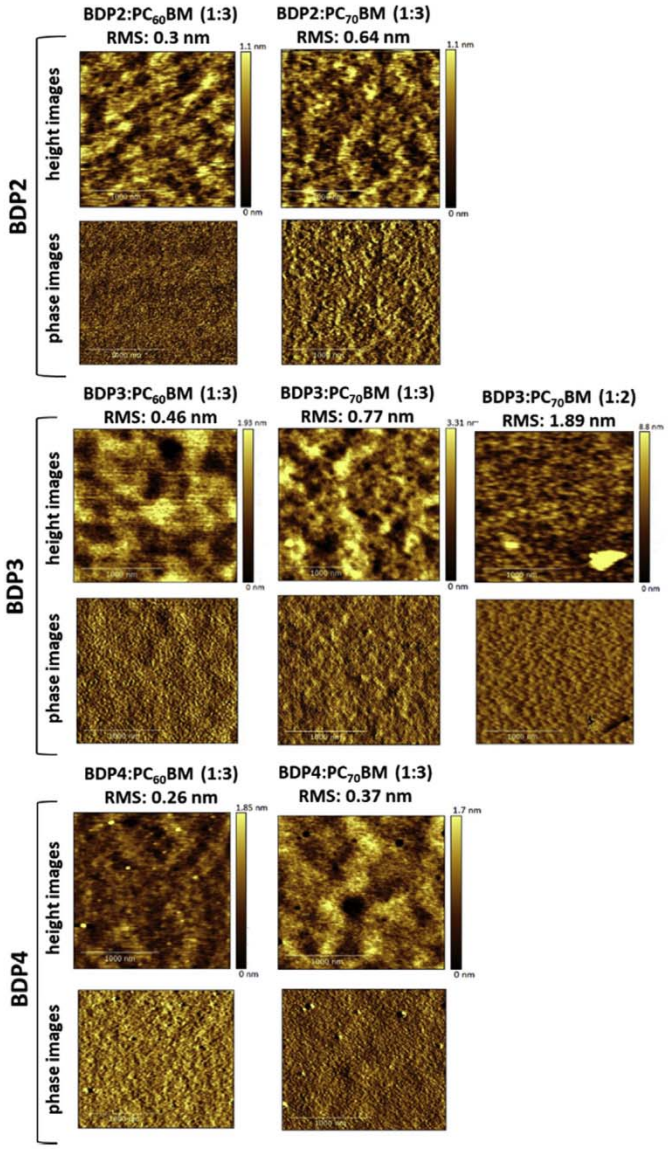

Fig. 5. AFM height images (top) and phase images (bottom) (2 μm vs 2 μm) of **BDP2**, **BDP3** and **BDP4** blended with $PC_{60}BM$ or $PC_{70}BM$.

topography may not represent the bulk morphology, and therefore it is difficult to correlate the efficiency with the AFM results.

4. Conclusions

In summary, we report the synthesis of a series of BODIPYs dyes, combining an electron-acceptor moiety at the *meso* position and an electron-donor styryl moiety linked to the backbone. The extremely fast reaction time, compared with the same synthesis procedure for other BODIPYs, and the photo-electrochemical properties of these BODIPYs (**BDP2-4**) makes them excellent donor material candidates for OPV cells. The BODIPYs reveal excellent thermal stability, strong spectral coverage, deep HOMO energy levels and good miscibility with $PC_{60}BM$ and $PC_{70}BM$. All BODIPY dyes act as electron-donors in a BODIPY:$PC_{60}BM$ blend but the corresponding solar cells exhibit efficiencies around 1% or below. However, they present very reasonable V_{OC} values. When combined with $PC_{70}BM$, the cells showed a large increase in their photovoltaic parameters. The maximum 2.79% PCE obtained is a very encouraging efficiency value and the open circuit current value (1.00) are amongst of the best achieved in OPV. We believe this could still be further enhanced, by optimization of the morphology and charge transport upon addition of additives or changing the contact layers. Such optimizations will be addressed in future works. This work demonstrates that BODIPY are promising photovoltaic materials if carefully planned and tailored.

Acknowledgements

The authors acknowledge the Fundação para a Ciência e a Tecnologia (FCT), Portugal, for the PhD research grant PD/BD/113702/2015 and postdoctoral research grant SFRH/BPD/103103/2014 and CNPq, Brazil for PhD research grant 232979/2014-6. The authors are also grateful for support from "The Coimbra Chemistry Centre" which is funded by the FCT, through the projects FCT UID/QUI/UI0313/2013 and COMPETE Programme (Operational Programme for Competitiveness) and also to IT support via the FCT-funded project UID/EEA/50008/2013.

Appendix A. Supplementary data

Supplementary data to this article can be found online at https://doi.org/10.1016/j.dyepig.2019.04.031.

References

[1] Zhang Y, Ye L, Hou JH. Precise characterization of performance metrics of organic solar cells. Small Methods 2017;1(8):1700159.
[2] Abdulrazzaq OA, Saini V, Bourdo S, Dervishi E, Biris AS. Organic solar cells: a review of materials, limitations, and possibilities for improvement. Part Sci Technol 2013;31(5):427–42.
[3] Lin Y, Li Y, Zhan X. Small molecule semiconductors for high-efficiency organic photovoltaics. Chem Soc Rev 2012;41(11):4245–72.
[4] Zhao X, Zhan X. Electron transporting semiconducting polymers in organic electronics. Chem Soc Rev 2011;40(7):3728–43.
[5] Cheng P, Zhan X. Stability of organic solar cells: challenges and strategies. Chem Soc Rev 2016;45(9):2544–82.
[6] Bucher L, Desbois N, Harvey PD, Sharma GD, Gros CP. Porphyrins and BODIPY as building blocks for efficient donor materials in bulk heterojunction solar cells. Solar RRL 2017;1(12):1700127.
[7] Panda MK, Ladomenou K, Coutsolelos AG. Porphyrins in bio-inspired transformations: light-harvesting to solar cell. Coord Chem Rev 2012;256(21):2601–27.
[8] Walter MG, Rudine AB, Wamser CC. Porphyrins and phthalocyanines in solar photovoltaic cells. J Porphyr Phthalocyanines 2010;14(09):759–92.
[9] Mishra A, Bäuerle P. Small molecule organic semiconductors on the move: promises for future solar energy technology. Angew Chem Int Ed 2012;51(9):2020–67.
[10] Heeger AJ, 25th Anniversary Article. Bulk heterojunction solar cells: understanding the mechanism of operation. Adv Mater 2014;26(1):10–28.
[11] Chen Y, Wan X, Long G. High performance photovoltaic applications using solution-processed small molecules. Acc Chem Res 2013;46(11):2645–55.
[12] Chen Y, Wan L, Zhang D, Bian Y, Jiang J. Modulation of the spectroscopic property of Bodipy derivates through tuning the molecular configuration. Photochem Photobiol Sci : Off J Europ Photochem Assoc Europ Soc Photobiol 2011;10(6):1030–8.
[13] Klfout H, Stewart A, Elkhalifa M, He H. BODIPYs for dye-sensitized solar cells. ACS Appl Mater Interfaces 2017;9(46):39873–89.
[14] Ziessel R, Ulrich G, Harriman A. The chemistry of Bodipy: a new El Dorado for fluorescence tools. New J Chem 2007;31(4):496–501.
[15] Ulrich G, Ziessel R, Harriman A. The chemistry of fluorescent bodipy dyes: versatility unsurpassed. Angew Chem Int Ed 2008;47(7):1184–201.
[16] Ni Y, Zeng L, Kang NY, Huang KW, Wang L, Zeng Z, et al. *Meso*-Ester and carboxylic acid substituted BODIPYs with far-red and near-infrared emission for bioimaging applications. Chem Eur J 2014;20(8):2301–10.
[17] Swavey S, Quinn J, Coladipietro M, Cox KG, Brennaman MK. Tuning the photophysical properties of BODIPY dyes through extended aromatic pyrroles. RSC Adv 2017;7(1):173–9.
[18] Hecht M, Fischer T, Dietrich P, Kraus W, Descalzo AB, Unger WES, et al. Fluorinated boron-dipyrromethene (BODIPY) dyes: bright and versatile probes for surface analysis. Chemistry 2013;2(1):25–38.
[19] Erten-Ela S, Yilmaz MD, Icli B, Dede Y, Icli S, Akkaya EU. A panchromatic boradiazaindacene (BODIPY) sensitizer for dye-sensitized solar cells. Org Lett 2008;10(15):3299–302.
[20] Xiao L, Wang H, Gao K, Li L, Liu C, Peng X, et al. A-D-A type small molecules based on boron dipyrromethene for solution-processed organic solar cells. Chem Asian J 2015;10(7):1513–8.
[21] Liao J, Zhao H, Xu Y, Cai Z, Peng Z, Zhang W, et al. Novel D–A–D type dyes based on BODIPY platform for solution processed organic solar cells. Dyes Pigments 2016;128(1):131–40.
[22] Liao J, Xu Y, Zhao H, Zong Q, Fang Y. Novel A-D-A type small molecules with β-alkynylated BODIPY flanks for bulk heterojunction solar cells. Org Electron

2017;49(1):321–33.
[23] Rousseau T, Cravino A, Ripaud E, Leriche P, Rihn S, De Nicola A, et al. A tailored hybrid BODIPY-oligothiophene donor for molecular bulk heterojunction solar cells with improved performances. Chem Commun 2010;46(28):5082–4.
[24] Lin H-Y, Huang W-C, Chen Y-C, Chou H-H, Hsu C-Y, Lin JT, et al. BODIPY dyes with [small beta]-conjugation and their applications for high-efficiency inverted small molecule solar cells. Chem Commun 2012;48(71):8913–5.
[25] Chen JJ, Conron SM, Erwin P, Dimitriou M, McAlahney K, Thompson ME. High-efficiency BODIPY-based organic photovoltaics. ACS Appl Mater Interfaces 2015;7(1):662–9.
[26] Liu W, Yao J, Zhan C. Performance enhancement of BODIPY dimer-based small-molecule solar cells using a visible-photon-capturing diketopyrrolopyrrole [small pi]-bridge. RSC Adv 2015;5(91):74238–41.
[27] Baran D, Tuladhar S, Economopoulos SP, Neophytou M, Savva A, Itskos G, et al. Photovoltaic limitations of BODIPY:fullerene based bulk heterojunction solar cells. Synth Met 2017;226(1):25–30.
[28] Jadhav T, Misra R, Biswas S, Sharma GD. Bulk heterojunction organic solar cells based on carbazole-BODIPY conjugate small molecules as donors with high open circuit voltage. Phys Chem Chem Phys 2015;17(40):26580–8.
[29] Li T-y, Benduhn J, Li Y, Jaiser F, Spoltore D, Zeika O, et al. Boron dipyrromethene (BODIPY) with *meso*-perfluorinated alkyl substituents as near infrared donors in organic solar cells. J Mater Chem 2018;6(38):18583–91.
[30] Arranja CT, Aguiar A, Encarnação T, Fonseca SM, Justino LLG, Castro RAE, et al. Double-tailed long chain BODIPYs - synthesis, characterization and preliminary studies on their use as lipid fluorescence probes. J Mol Struct 2017;1146(1):62–9.
[31] Boens N, Qin W, Baruah M, De Borggraeve WM, Filarowski A, Smisdom N, et al. Rational design, synthesis, and spectroscopic and photophysical properties of a visible-light-excitable, ratiometric, fluorescent near-neutral pH indicator based on BODIPY. Chemistry 2011;17(39):10924–34.
[32] Boens N, Leen V, Dehaen W. Fluorescent indicators based on BODIPY. Chem Soc Rev 2012;41(3):1130–72.
[33] Xu J, Zhu L, Wang Q, Zeng L, Hu X, Fu B, et al. *Meso*-C6F5 substituted BODIPYs with distinctive spectroscopic properties and their application for bioimaging in living cells. Tetrahedron 2014;70(35):5800–5.
[34] Galangau O, Dumas-Verdes C, Méallet-Renault R, Clavier G. Rational design of visible and NIR distyryl-BODIPY dyes from a novel fluorinated platform. Org Biomol Chem 2010;8(20):4546–53.
[35] Banfi S, Nasini G, Zaza S, Caruso E. Synthesis and photo-physical properties of a series of BODIPY dyes. Tetrahedron 2013;69(24):4845–56.
[36] Loudet A, Burgess K. BODIPY dyes and their Derivatives: syntheses and spectroscopic properties. Chem Rev 2007;107(11):4891–932.
[37] Lanzani G, Nisoli M, De Silvestri S, Tubino R. Femtosecond vibrational and torsional energy redistribution in photoexcited oligothiophenes. Chem Phys Lett 1996;251(5):339–45.
[38] Li L, Huang Y, Peng J, Cao Y, Peng X. Enhanced performance of solution-processed solar cells based on porphyrin small molecules with a diketopyrrolopyrrole acceptor unit and a pyridine additive. J Mater Chem 2013;1(6):2144–50.
[39] Bernède JC. Organic photovoltaic cells: history, principles and techiques. J Chil Chem Soc 2008;53(403):1549–64.
[40] JRA J, Jenny N. Factors limiting device efficiency in organic photovoltaics. Adv Mater 2013;25(13):1847–58.
[41] Ilmi R, Haque A, Khan MS. High efficiency small molecule-based donor materials for organic solar cells. Org Electron 2018;58(1):53–62.
[42] Zhang F, Zhuo Z, Zhang J, Wang X, Xu X, Wang Z, et al. Influence of PC60BM or PC70BM as electron acceptor on the performance of polymer solar cells. Sol Energy Mater Sol Cell 2012;97(1):71–7.